High Temperature Mechanical Testing of Metals

58

Birgit Skrotzki, Jürgen Olbricht, and Hans-Joachim Kühn

Contents

Abstract

Performing mechanical tests at high temperatures is a nontrivial issue: Compared to room temperature testing, additional phenomena like time-dependent deformation processes and oxidation effects raise the complexity of the material's response, while more sophisticated test setups and additional control parameters

B. Skrotzki (✉) · J. Olbricht · H.-J. Kühn
Bundesanstalt für Materialforschung und -prüfung (BAM), Berlin, Germany
e-mail: birgit.skrotzki@bam.de; juergen.olbricht@bam.de; kuehn_hans-joachim@t-online.de

C.-H. Hsueh et al. (eds.), *Handbook of Mechanics of Materials*,
https://doi.org/10.1007/978-981-10-6884-3_44

increase the number of potential sources of error. To a large extent, these complications can be overcome by carefully following all recommendations given in the respective high temperature testing standards, but more comprehensive background information helps to identify points of specific importance in particular test campaigns. In this chapter, an overview is given on general high temperature testing issues like the appropriate choice of experimental equipment and key aspects of temperature measurement. In subsequent sections, the major static and dynamic high temperature test methods are reviewed and their special features, as compared to testing at room temperature, are highlighted based on example data sets. Influences of specimen size and environmental effects are shortly outlined in a concluding section. In the whole chapter, a focus is set on testing of "classical" metallic high temperature materials, but many considerations are equally valid for testing of intermetallics, composites, and high temperature ceramics.

1 Symbols

Note that the designation may be different from those used in the standards for the sake of continuous consistency in this chapter.

a	crack length
A	elongation after fracture
E	Young's modulus
E_C	modulus on unloading, following a peak compression stress
E_T	modulus on unloading, following a peak tensile stress
K_{max}	maximum stress intensity
K_{min}	minimum stress intensity
K_{th}	threshold value of stress intensity factor
ΔK	stress intensity factor range
L_e	elongation after fracture
n	stress exponent (Norton exponent)
N	cycle number
N_{20}	number of cycles to 20% stress drop
N_f	number of cycles to failure
Q_c	apparent activation energy for creep
R	gas constant
$R_{p0.2}$	0.2% yield strength
R_m	tensile strength
R_ε	strain ratio
R_σ	stress ratio
t	time
T	temperature
T_{max}	maximum temperature
T_{mean}	mean temperature

T_{min}	minimum temperature
T_s	melting temperature
$\dot{T}$	temperature rate
ΔT	temperature range
Z	reduction of area
φ	phase angle between strain and temperature
ε	strain
ε_0	spontaneous time-independent strain during loading in a creep test
ε_a	strain amplitude
ε_c	creep strain
ε_e	elastic strain
ε_i	anelastic time-independent initial strain during loading in a creep test
ε_{in}	inelastic strain
ε_m	mechanical strain
ε_{max}	maximum strain
ε_{min}	minimum strain
ε_p	plastic strain
ε_t	total strain
ε_{th}	thermal strain
$\Delta\varepsilon_p^t$	plastic strain range, determined by tangential method
$\Delta\varepsilon_p^w$	plastic strain range, determined from width of hysteresis curve
$\Delta\varepsilon$	strain range
$\Delta\varepsilon_c$	elastic strain range
$\Delta\varepsilon_m$	mechanical strain range
$\Delta\varepsilon_p$	plastic strain range
$\Delta\varepsilon_t$	total strain range
$\dot{\varepsilon}$	strain rate
$\dot{\varepsilon}_{min}$	minimum creep rate
σ	stress
σ_{max}	maximum stress
σ_{min}	minimum stress
σ_{engg}	engineering stress
σ_{mean}	mean stress
σ_{RC}	relaxed stress in compression during hold time
σ_{true}	true stress
$\Delta\sigma$	stress range

2 Introduction

The design of mechanically loaded components, e.g., for applications in mechanical engineering, in automotive industry (exhaust manifolds, turbocharger components), in aerospace (turbine blades and disks), or in power plant technology (heat exchanger, boiler components), requires knowledge of the material behavior at high temperature. These components may be subjected to static, quasi-static, cyclic, or thermal loads, or a combination of two or more. Design data are commonly derived from elevated tensile/compression tests, relaxation tests, stress rupture/creep tests, low cycle fatigue (LCF) tests, and crack propagation tests in a temperature regime, which fully covers the envisaged service temperatures. The temperature dependence of Young's modulus is also often determined, either by static or by dynamic methods. In recent years, combined loadings such as the superposition of thermal and mechanical cycles (thermomechanical fatigue (TMF)) gained in importance for design procedures. Another example is the superposition of low and high cycle fatigue (HCF).

The safe dimensioning of components essentially requires the reliable determination of characteristic values of material properties. The identification of these material properties at high temperature represents a particular challenge. This chapter will therefore focus on the specific features and requirements of testing at high temperature. A basic knowledge of the test procedures at room temperature is presumed. Due to space limitations, only testing of regular specimens will be discussed here. For the topic of component testing, the reader is referred to dedicated publications.

The reliable determination of the characteristic values for material properties at room temperature as well as at high temperature imperatively requires the strict observation of the respective test standards, which define the experimental requirements and allowable tolerances that need to be fulfilled to trust in any obtained result. However, while each individual test type clearly has its own peculiarities, a number of aspects with general importance in high temperature testing can be identified, as will be discussed below. Experience has shown that the temperature measurement and the heating method are key factors in high temperature testing due to their substantial influence on the obtained properties. Before any test, it first needs to be verified which heating methods (cf. Sect. 3) are permitted by the test standard and how test parameters can be kept in the given tolerance range. Compared to room temperature testing, this requires considerable effort as well as additional cost.

Besides heating method, the temperature measurement represents the largest challenge (cf. Sect. 4). Different measuring techniques (contact or non-contact measurement), effect of heating method on temperature measurement, measuring position, as well as shortcomings in the measuring setup and in calibration are potential sources of error. The temperature measurement shall be carried out with highest accuracy and, if possible, ensured by complementary methods.

Furthermore, special attention must be paid to all parts of the load train since they must be capable of transferring the test loads at high temperature without exceeding the limits of the permitted bending strain. Depending on the test temperature, it is sometimes not easy to identify suitable materials. The materials must provide a sufficient oxidation and scaling resistance to avoid blockade of movable parts that would affect the alignment of the load train. Surfaces which contribute to alignment have to be checked frequently and parts have to be reworked to remove emerging oxide layers. Screwed joints in the load train may easily fuse inseparably or get jammed by creep or oxidation of threads. The use of suitable high temperature mold release agents such as boron nitride or MoS_2 may help sometimes.

If parts of the clamping system are subjected to high temperatures (which is often the case when using resistance furnaces or environmental chambers), these parts have to be manufactured from high temperature materials which show at least a comparable high temperature strength and creep resistance as the material to be tested. Such “hot” grips are often used in elevated tensile and in creep tests because they provide a homogeneous temperature distribution along the gauge length.

Two basic grip activation principles are available: either mechanical or hydraulic clamping systems may be used. Mechanical clamping devices, such as thread or wedge systems, mostly do not allow complying with the tight bending limits required for LCF and TMF tests. Generally, hydraulic collet grips ensure the highest reproducibility of gripping the test specimens and offer reasonably priced specimen geometry (cylinder shaft). In addition, their working principle ensures that any changes in clamping force due to differences in thermal expansion or due to creep will securely be impeded. However, hydraulic grips stringently require water-cooling for protection of oil and sealings (“cold” grips). Therefore, this grip type is often used together with induction heating within the gauge length, which only allows a homogeneous temperature distribution along a rather short range of the specimen. Compared to “hot” grips, the gripping sections of the test pieces remain rather cold due to the water-cooled collet grips, resulting in larger axial temperature gradients which make it more difficult to maintain the limits required by the standards. The compliance with the temperature gradient limits is mandatory and must be verified for each individual test temperature.

On the other hand, cooled grips act as heat sinks and ensure rapid cooling of specimens when the heating power is reduced. High cooling rates can then be achieved, which is sometimes desirable for non-isothermal tests. “Cold” collet grips are therefore ideal for TMF tests.

The strain measurement demands adjustment to the high test temperature because conventional methods/sensors used at room temperature are limited to very moderate operation temperatures. High temperature contact extensometers use ceramic extension rods. They require either air or water-cooling to prevent damage of the sensor and to avoid drift during heating or during thermal cycling. Non-contact solutions are laser or video based or employ digital image correlation (DIC) techniques. They are usually applied for short tests or for tests, which do not require closed-loop control by the strain signal. Assessment of the data may be difficult due to heat haze, which may cause noise and thus affect the accuracy and resolution of the sensor.

Attention should also be paid to the calculation of strain. Not all of the standards explicitly define the reference value for the calculation of strain and stress. It is clear for tests at room temperature that the specimen dimensions (diameter, width, height) and the initial gauge length of the extensometer at room temperature are used. However, in high temperature testing, it needs to be agreed on whether the base values at room temperature or at testing temperature are used. The different alternatives will be shortly outlined in Sect. 6.

Finally, the loading rate becomes more important at high temperature testing, because with raising temperature creep processes are increasingly activated and thus the stress-strain behavior becomes increasingly time dependent. The effect will be exemplified in Sect. 6 for tensile tests but needs to be considered in all test types that imply preset loading rates.

3 Heating Methods

Common devices for heating the specimen are radiation furnaces, induction heaters, and direct resistance heating units. Radiation furnaces (Fig. 1a) are commercially available from many different suppliers. They have one or more heating zones that are triggered by a controller using the feedback from thermocouples directly attached to the specimen at one or more locations (depending on gauge length).

Lamp furnaces (Fig. 1b) provide radiant heat from quartz lamps mounted in reflective and cooled housings. The furnace uses multiple lamps, with each focusing its energy on a limited area of the test piece. Therefore, good thermal conductivity of the specimen is required to establish uniform temperature distribution. Lamp furnaces can achieve much faster heating and cooling rates than radiation furnaces.

Induction heaters establish an electromagnetic field by an induction coil that surrounds the test piece (Fig. 1c). The geometry of the coil depends on the specimen geometry. The coils are usually homemade. The number and spacing of the loops are usually determined empirically, which requires a certain experience for best performance.

A less frequently used method is heating by direct resistance heating. The technique is based on passing an electric current directly through the specimen from one end to the other (Fig. 1d). This requires a powerful current source but also an electrical insulation of the specimen grips to the testing machine. Specimens with a uniform cross section are more suitable than nonuniform ones as a more uniform temperature distribution is obtained when the current density remains constant along the gauge length. Due to cooling by the grips, the resulting temperature distribution is anyway nonuniform (following a parabolic function) along the gauge length (Fig. 2). Therefore, temperature measurement in the central part, at the location where the highest temperature is expected, is required. Because of the high current that passes through the specimen, the temperature measurement is more challenging when this heating method is used. Thermocouples cannot be welded directly to the specimen, since the heating current would affect the measured thermoelectric voltage. The use of mantle thermocouples is possible, but their more sluggish behavior must be taken into account for the feedback control.

Irrespective of the used heating method, the uniformity of the temperature along the gauge length has to be verified on a dummy specimen with a similar geometry than the actual specimen to be tested. Therefore, the temperature is mapped with multiple thermocouples on different locations in the reduced section of the specimen (Fig. 3).

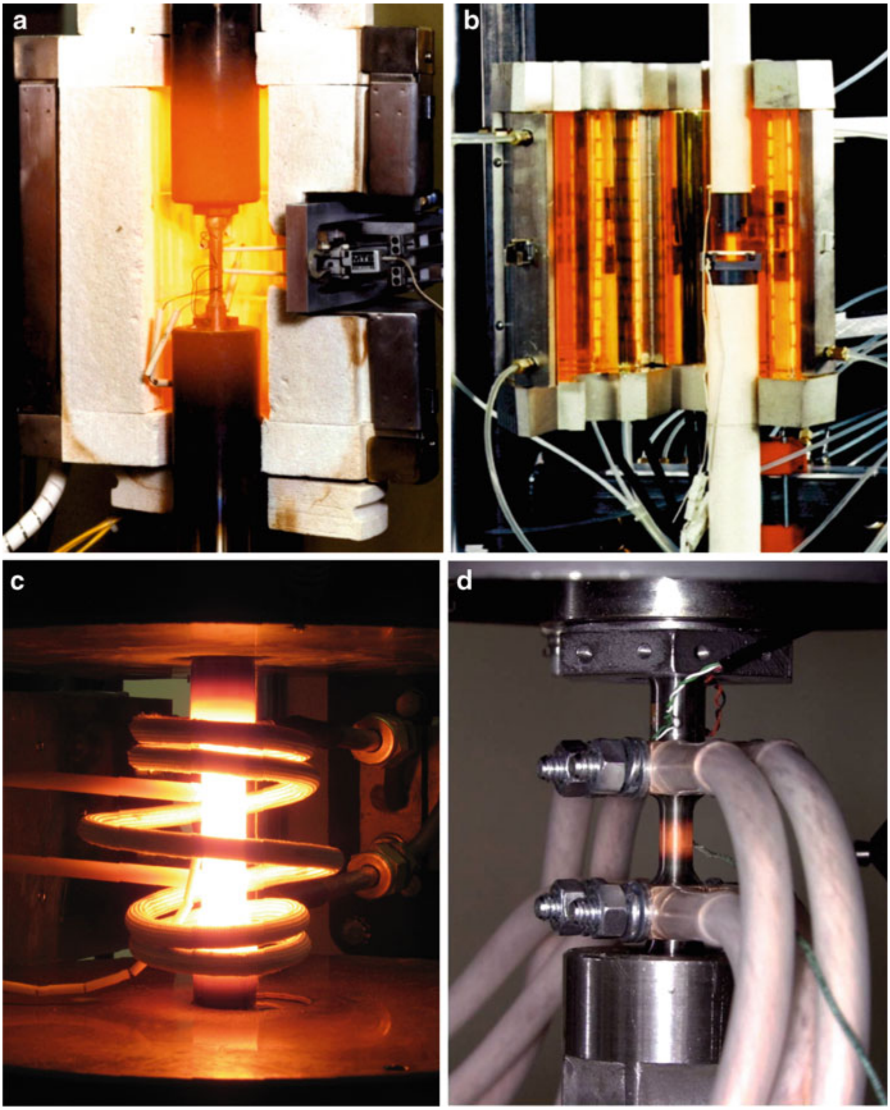

Fig. 1 Heating devices for mechanical testing. (**a**) Radiation furnace, (**b**) lamp furnace, (**c**) induction heating device, (**d**) direct resistance heating system

4 Temperature Measurement

Besides load and deformation measurement, the correct determination of the specimen temperature represents a particular challenge in materials testing. The peculiarities are the different calibration procedures, which are applied depending on the

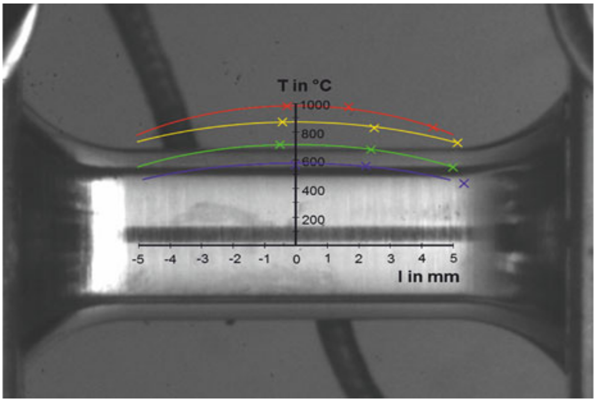

Fig. 2 Parabolic temperature profiles determined in the gauge length of a specimen heated by direct resistance

Fig. 3 Dummy specimen instrumented with multiple thermocouples at different locations to determine axial and circumferential temperature gradients

chosen measurement method, and variable disturbances which are often not easy to quantify. In addition, different measurement procedures and a multitude of temperature sensors are available which must be chosen depending on test type (standard), maximum test temperature, and test time.

The standards for materials testing at elevated temperature favor two options for temperature calibration:

(a) Calibration of the complete measuring chain
(b) Separate calibration of sensors (e.g., thermocouple) and indicating device

Procedure (a) is more complex, because it has to be carried out separately at each testing machine. Deviations should be smaller as compared to (b), because the complete measuring chain including all plug connections remains unchanged after calibration. Procedure (b) is more universal though, because temperature sensors can be calibrated centrally and interchanged between testing machines. Both methods disregard contacting aspects (sensor to specimen), although contacting may result in considerable errors in temperature measurement.

In contrast to measurements of force or length changes, the temperature measurement is difficult to verify by simple methods. The force measurement can be checked before a test by using weights and the length change measurement by help of the crosshead displacement (while applying the extensometer to a cut specimen). After the test, Young's modulus is calculated and its plausibility is reviewed. For the temperature measurement however, the only option before the test is to test the indicating device by feeding a thermoelectric voltage. The contacting problem is excluded.

Therefore, all options for checking the temperature measurement should be utilized. A reference specimen (with known thermal expansion and Young's modulus $E = \mathrm{f}(T)$) can be used to verify the temperature measuring chain before starting a test series. Then, the thermal length change and Young's modulus at room temperature and at testing temperature can be determined before each test. With these results, the temperature measurement can be verified relatively in direct comparison within the test series as long as the scatter of Young's modulus and of the thermal expansion values is small within the sample material, but no absolute check is possible. Under ideal conditions, temperature deviations of $\geq$15 K at best can be detected by such comparisons. If applicable, characteristic temperatures such as known transformation temperatures (e.g., ferrite to austenite transformation, magnetic transformation in iron/steel) can also be used to check the accuracy of the temperature measurement as long as they leave traces (like short hold points during heating) in the test data.

Temperature measuring methods with direct contact of the sensor to the specimen surface as well as non-contacting methods are available. The most common techniques in materials testing are pyrometers (non-contact) and thermocouples (contact).

Non-contact measurements offer some clear advantages: their response time is very low and the measuring point on the specimen is neither affected mechanically (crack initiation due to stress concentrations) nor thermally (cold spot due to heat conduction through the sensor cable). Electromagnetic fields (resulting from induction heating) and electric currents (resulting either from potential drop measurements to document crack propagation or from direct resistance heating) do not influence the temperature measurement. Despite these merits, pyrometers are rarely used. Compared to thermocouples, the pyrometer measurement has the large disadvantage of limited accuracy and lower long-term stability in mechanical testing applications. The reason is mainly a changing emission coefficient with increasing oxidation and/or changes in surface quality by cyclic loading, resulting in an altered temperature indication. Deviations of more than 100 K compared to a reference thermocouple were demonstrated [1].

Most temperature measurements in materials testing are therefore performed using thermocouples. Besides ready-made mantle thermocouples, thermocouples with bare wires are used as well, which can be tied or spot-welded to the specimen. Unfortunately, any contacting measurement results in an impact at the measuring point by the temperature sensor. Spot welding of the thermocouple wires to the specimen leads to optimum heat coupling of sensor and specimen, but in many cases it results in a surface damage of the specimen, which may promote crack initiation under cyclic loading. For some materials, even tying of a thermocouple results in premature failure. In such cases, the thermocouples are attached to the end of the specimen gauge length, in the transition radius to the specimen head. This procedure requires further pretests to relate the temperature at the radius to the temperature of the gauge length.

Base metal thermocouples should not be reused without clipping back to remove the wire exposed to the hot zone to avoid measuring errors. Noble-metal thermocouples may contaminate due to direct contact with the test piece, which also causes errors due to drift. They should be annealed periodically and checked for calibration. Care should be taken to keep the thermocouples clean prior to exposure and during use at elevated temperatures.

Many commercially available temperature measuring devices were designed for quasi-static temperature measuring tasks only. Often, similar devices are used for TMF testing also due to cost reasons. However, in TMF tests, temperatures need to be measured under high temperature rates ($\dot{T}$ up to 50 K/s) and within wide temperature ranges. Unsuitable temperature measuring devices may result in unacceptable amplitude and phase errors. Therefore, the dynamic behavior of the used temperature measuring chain has to be checked.

The dynamic performance will also depend on the utilized data acquisition system, but most modern systems in state-of-the-art testing machines can simultaneously acquire several channels at sample rates of >1 kHz. They are at least 50 times faster than conventional temperature measuring devices and, therefore, well qualified for TMF testing. However, they should be integrated in the verification of the whole measuring chain.

5 Young's Modulus

Young's modulus, E, can be determined by different test methods. The tensile test represents a commonly used procedure, because there Young's modulus is required anyway to determine the characteristic material property values. However, the value determined in tensile test is in many cases defective due to a poor alignment of the load train and single side strain measurement. In the relevant standards, this value is therefore not designated as Young's modulus but as "straight-line portion of the stress-strain curve" [2], with the strain being determined by extensometer measurement.

Testing machines used for LCF and TMF testing must meet the requirements with respect to bending [3] which are stricter than those for tensile tests. This results in lower scattering of Young's modulus values than in tensile tests. In LCF tests, Young's modulus is determined in the first quarter of the stress-strain cycle of the test [4]. For TMF tests, the determination of the temperature-dependent Young's modulus ($E = \mathrm{f}(T)$) is part of the pretest procedure to check the correct test setup [1, 5, 6] (cf. Sect. 10).

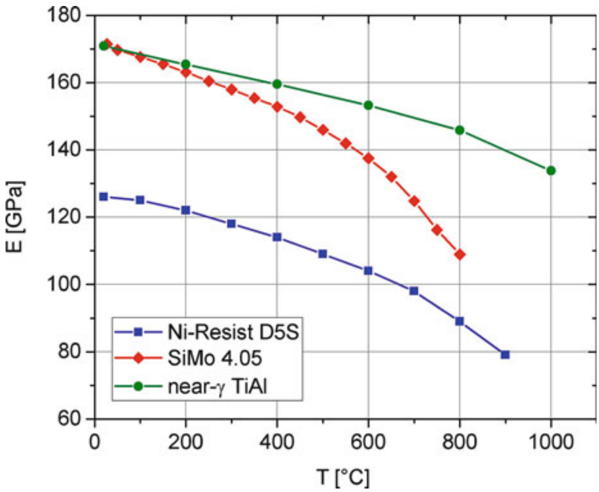

Fig. 4 Temperature-dependent Young's moduli of austenitic heat-resistant cast iron Ni-Resist D5S, ferritic heat-resistant cast iron GJS X SiMo 4.05, and of an intermetallic titanium aluminide determined by the resonance method

Young's modulus can be determined by dynamic methods as well, e.g., by the resonance method [7] or by ultrasound. The resonance method is based on measuring the resonance frequencies of a free hanging specimen after excitation, e.g., by a piezo actuator. It allows the temperature-dependent determination of Young's modulus with only one specimen with a measurement uncertainty of less than 1% [8]. Young's modulus is calculated from the specimen geometry, the mass, and the measured resonance frequencies.

The method is suited for homogeneous and isotropic metallic and ceramic materials. In Fig. 4, the temperature-dependent evolution of Young's modulus, E, of a ferritic (diamonds) and an austenitic (squares) heat-resistant cast iron and of an intermetallic near-γ titanium aluminide alloy (circles) is shown; all curves have been determined by the resonance method. The elastic constants of anisotropic materials (e.g., single crystals) may similarly be determined, but higher calculation efforts are then required [9].

6 Elevated Temperature Tensile Tests

Basic material properties like the yield point and maximum strength of a material under static loading are typically determined at room temperature, but the corresponding values at operating temperatures are equally important to analyze component behavior in the case of high temperature materials.

Elevated temperature tensile tests (often referred to as *hot tensile tests* also) generally allow determining the same material parameters like standard tensile tests do. In particular, the ultimate tensile strength, the elongation after fracture, and the reduction of area are usually analyzed. The main focus, however, will often be set on the yield strength as long as temperatures are kept in the technologically relevant range, where elastic and plastic deformation regimes can still be reasonably

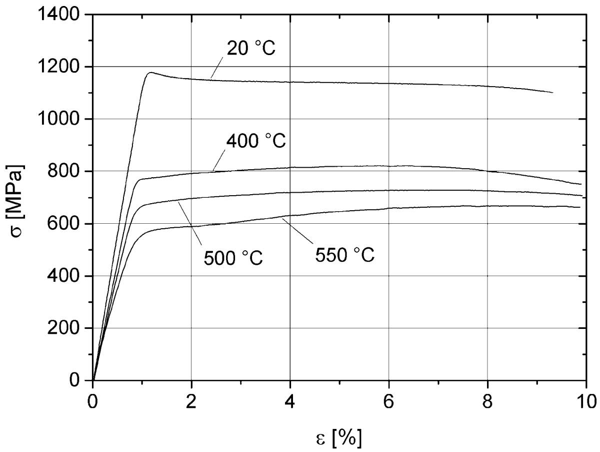

Fig. 5 Tensile behavior of titanium alloy Ti-6242 at different elevated temperatures (tests conducted at $\dot{\varepsilon} = 10^{-3}\ \mathrm{s}^{-1}$ and discontinued at strains of about 10%)

separated. In Fig. 5, example curves are given for the high temperature tensile behavior of a titanium alloy. Similar to the room temperature test, the curves obtained at 400 °C to 550 °C exhibit distinct elastic ranges at strains below 1%, followed by plastic deformation with little variation in stress.

Metals and alloys typically exhibit significant strength reductions with increasing temperature, accompanied by a simultaneous increase in ductility. This opposing trend of strength and ductility is illustrated in Fig. 6, in which data of an austenitic cast iron is shown. As frequently observed, the tensile properties of this material change only gradually when the temperature is increased up to a certain limit (about 500 °C in Fig. 6). On further increase of temperature, a range of much stronger property changes follows, eventually leading to very low strengths, which would impede the use of the material in most technical applications.

With regard to testing equipment, the aspects mentioned in previous sections apply and adequate heating, gripping, temperature measurement, and extensometry equipment must be used in accordance to the relevant standards for elevated temperature tensile tests (e.g., [10, 11]). The heating system needs to provide a sufficiently large hot zone, since hot tensile tests often lead to considerable elongation of specimen due to the increased ductility of the materials. Small furnaces and induction heating systems are therefore often inappropriate. Alternatively, environmental chambers can be used. They can help to achieve low temperature gradients in the specimens, but most models operate up to about 500 °C only and they require grips that can be fully placed into the hot zone. The classical specimen geometries known from room temperature tests shall be used, especially with respect to the aspect ratio of the gauge section. Extension of the specimen shoulders can be helpful if gripping outside a furnace is needed (cold grips), but special attention should then be paid to checking whether the alignment and temperature gradient requirements given in the standards are still met.

Two issues deserve special attention when comparing results of room temperature and elevated temperature tensile tests or intercomparing elevated temperature test

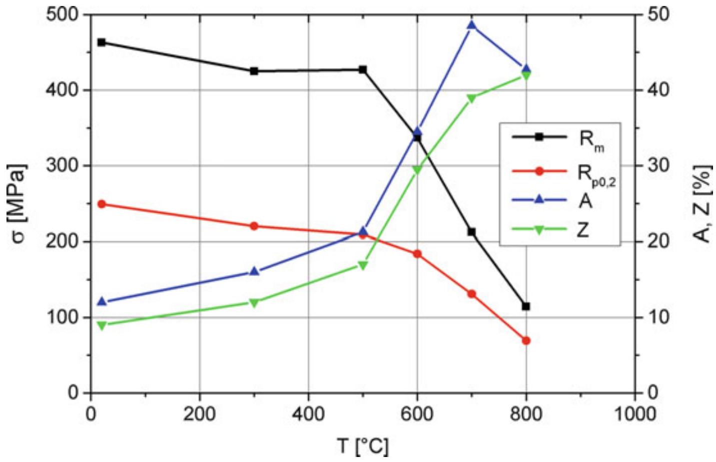

Fig. 6 Temperature dependence of yield strength ($R_{p0,2}$), ultimate tensile strength (R_m), elongation after fracture (A), and reduction of area (Z) of the austenitic heat-resistant cast iron Ni-Resist D5S

results. First, it needs to be considered that various methods for determining the extensometer gauge length L_e are used in practice, which may lead to little differences in the obtained test results. The nominal gauge length of any extensometer increases slightly upon heating to test temperature due to thermal expansion, and four common strategies for handling this effect are outlined in [10]. The easiest but most inaccurate approach is to ignore the thermal expansion and work with the room temperature gauge length, which may be acceptable in case of lower test temperatures. Alternatively, a compensation of the effect can be achieved by

– Mounting the extensometer to the test piece at room temperature with an adjusted negative preset, which will exactly be compensated by the thermal expansion that develops during heating.
– Mounting the extensometer, set to its nominal gauge length, after the test piece was heated to test temperature (only applicable when adequate testing equipment is available).
– Mounting the extensometer, set to its nominal gauge length, to the test piece at room temperature. A corrected gauge length (nominal length plus thermal expansion) is used for the calculation of the extension.

The second issue that may complicate comparisons of room temperature and elevated temperature test results is related to time-dependent deformation processes in the materials (see Sect. 7 for further details). These processes require thermal activation and thus become increasingly important the higher the test temperatures are. Their strain contribution results in a growing elongation of the specimen the longer it is kept under tension due to diffusion-controlled dislocation motion in the microstructure. As a result, the test speed generally has a stronger influence on the obtained tensile properties in hot tensile tests than observed at room temperature,

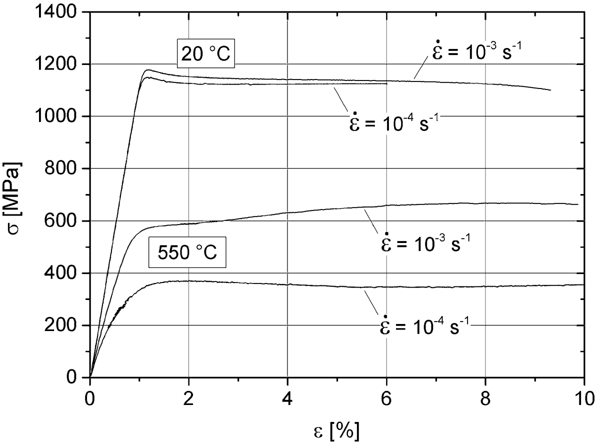

Fig. 7 Influence of strain rate on the tensile behavior of titanium alloy Ti-6242 at room temperature and 550 °C (tests discontinued at strains of about 10%)

as is exemplified in Fig. 7 for a titanium alloy. While the tensile curves obtained at room temperature and different strain rates show little difference, similar tests at 550 °C yield results with an almost 300 MPa deviation. The slow deformation at the lower strain rate of $\dot{\varepsilon} = 10^{-4}\ \mathrm{s}^{-1}$ promotes the generation of strain via diffusion-controlled processes. As a result, lower stresses are sufficient to reach the specified total deformation per time unit.

Actual standards (e.g., [10, 11]) consider significantly lower test speeds, compared to their room temperature counterparts, especially for the first stage of the test up to the determination of the yield strength. This tendency to a more quasi-static loading condition leads to lower, and thus more conservative, strength values in the elevated temperature test, but these do not necessarily coincide with the real loading conditions in an application and direct comparison with room temperature results is then not straightforward. To enable intercomparisons under similar conditions, either room temperature tests at reduced speeds [2, 12] or accelerated tests at elevated temperature [10] are suggested in the standards.

7 Creep, Creep Rupture, and Stress Rupture

7.1 Definitions

Creep is defined as a time-dependent deformation, which develops under a given load at a sufficiently high temperature. It is commonly accepted that creep processes become relevant at temperatures above 0.4 to 0.5 T_s (T_s is the melting temperature in K). They are caused by climb of dislocations, which induce time-dependent plastic deformation. Creep is a subtle process, which does not come to rest as long as an external load is operating. The creep strain is a function of applied stress, temperature, time, material, and material condition. In a *creep test*, creep strain is measured and the creep rate $\dot{\varepsilon} = d\varepsilon/dt$ is calculated. The load is sufficiently low so that creep strains remain small and no fracture occurs. In a *creep rupture test*, the applied load is higher, the specimen deforms progressively, and, besides creep strain, the time to fracture is measured. In a *stress rupture test*, no strain measurement is being made but the time to fracture is measured.

The measured data serve defining the load-carrying ability of a material and support selecting the appropriate material for parts for service at elevated temperatures. Creep tests and rupture tests complement each other in this process.

7.2 Experimental Setup and Conduction of Tests

The test rigs used for creep and rupture tests are less complex than tensile or fatigue testing machines. It is a static test and the load (i.e., a weight in standard setups) is applied via a lever arm to the test piece. However, the long testing time represents a challenge because the testing parameters have to remain constant possibly for many years.

It is usual practice in an engineering creep test to maintain the load (i.e., force) constant throughout the test. This means that the true stress increases during the test due to elongation of the specimen and reduction of its cross section. Nonetheless, the initial (engineering) stress applied to the specimen is usually reported. Deviations between the true stress, σ_{true}, and the engineering stress, σ_{engg}, become relevant only at strains exceeding 10%:

$$\sigma_{true} = \sigma_{engg}(1 + \varepsilon), \tag{1}$$

with ε being the engineering strain.

In principle, establishing constant stress conditions is feasible using an adjusted and bent lever arm, but this setup is rarely used. It is found that the onset of the tertiary regime (see below) is largely delayed under constant stress as compared to constant force.

The testing machine must be able to apply the force as axially as possible with a minimum of bending strain. The test piece is heated up by an electric resistance or radiation furnace. The temperature is measured by a sufficient number of thermocouples (cf. [13, 14]) along the gauge length of the test piece. Creep and rupture tests are long-term tests ranging from a couple of hundred hours to several years.

The deformation of the test piece is measured by an extensometer system. The sensitivity and accuracy of the system should match the expected deformation. A creep test, e.g., requires an extensometer with a higher resolution than a creep rupture test due to the smaller deformation. The extensometer should be attached directly to the specimen to the reduced portion and not to the grips, which might become difficult if the specimens are very small. Measuring the deformation on opposite sides and averaging the signal increases the accuracy as compared to measurements on only one side of the specimen.

It is recommended to use test pieces of circular cross section [13, 14]. Tensile test specimen geometries are generally suitable. However, the reduced section should

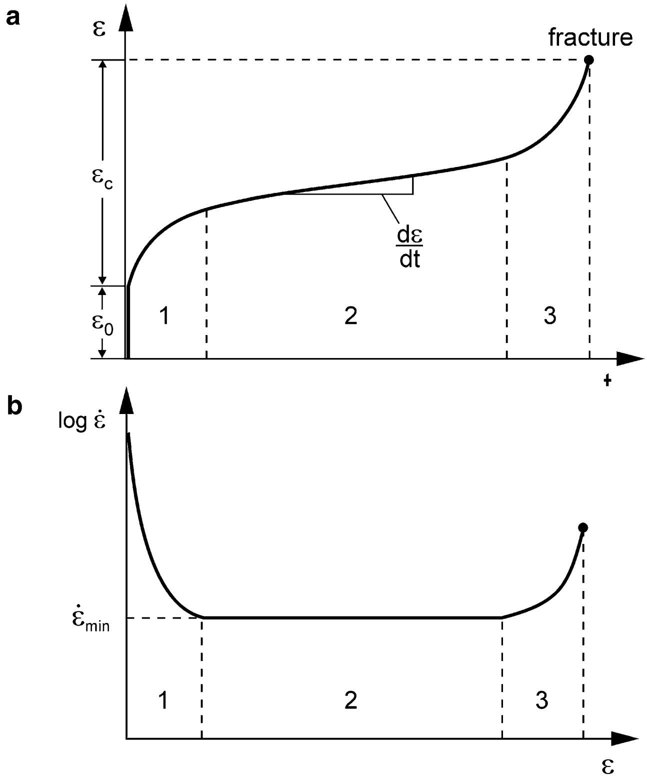

Fig. 8 (**a**) Ideal creep rupture curve showing primary, secondary, and tertiary creep regime. (**b**) Creep rate versus creep strain

have a larger ratio of length to diameter to increase the accuracy of the strain measurement. The specimen diameter should be large enough to contain a reasonable large number of grains in the cross section.

The specimen is heated to test temperature without overshooting. A small load (up to approximately 10%) may be applied before and during heating to improve axiality. The temperature is held constant for at least 1 h (and maximum 24 h) to establish thermal equilibrium. The load is applied avoiding any torsion, bending, or shock forces. The creep strain measurement starts at complete application of full force. The instantaneous strain, which results up to full loading, is recorded as well. The total strain ε_t is the sum of the spontaneous, time-independent strain ε_0 and the time-dependent creep strain ε_c (Fig. 8a). ε_0 is composed of an elastic component $\varepsilon_e = \sigma/E$ and an anelastic, time-independent initial strain ε_i [15]:

$$\varepsilon_t = \varepsilon_0 + \varepsilon_c = \varepsilon_e + \varepsilon_i + \varepsilon_c \tag{2}$$

For the sake of convenience, the creep strain ε_c is called ε in the following.

7.3 Creep and Creep Rupture Testing

The idealized shape of a creep rupture curve is shown schematically in Fig. 8a as (creep) strain versus time. The ideal creep curve is only observed for pure metals and some solid solution alloys. Technical alloys and especially particle hardened alloys may show considerable deviations from the ideal shape (cf. Fig. 9a and b).

The primary creep regime (1) is characterized by a rapidly decreasing strain (creep) rate $\dot{\varepsilon} = d\varepsilon/dt$. In the secondary creep regime (2), the creep rate is constant. The creep rate quickly increases in the tertiary creep regime (3) due to damage processes such as formation of creep pores and cracks. The curve ends with fracture of the test piece. Creep ductile materials show considerable necking.

It is often preferable to represent creep data as log strain rate versus strain (Fig. 8b), because the strain rate directly represents the material's response to loading and the strain is a measure for the deformation state. Figure 9c and d illustrates that creep rate versus creep strain diagrams of technical materials show a different shape than the ideal curve. Note that the minimum of the creep rate is rather distinct as compared to the wide plateau in Fig. 8b.

The creep rate is an important design parameter derived from the creep curve. Information such as the stress to produce a certain creep rate is derived from the tests. The creep rate is a strength measure: the lower the creep rate, the higher the creep strength. The creep strength characterizes the resistance of a material to deformation.

The strain rate depends on the applied stress and temperature. Its stress dependence can be described by the well-known phenomenological equation:

$$\dot{\varepsilon} = A \cdot \exp\left(-\frac{Q_c}{RT}\right) \cdot \sigma^n, \qquad (3)$$

where A represents a constant, Q_c the apparent activation energy for creep, R the universal gas constant, T the temperature, σ the creep stress, and n the stress exponent (also called Norton exponent). In the case of simple model materials, Eq. (3) can be interpreted in terms of the steady-state creep approach. It is based on the physical view that a strain hardening process (e.g., increase of dislocation density) is balanced by a time softening process (e.g., climb-controlled dislocation annihilation) resulting in a dynamically steady microstructure (e.g., with constant dislocation density). In such systems, the stress and temperature dependence of the creep rate can be rationalized by the stress and temperature dependence of the simple elementary processes. Then, an activation energy of creep is often found, which corresponds to that for self-diffusion and a stress dependence of the creep rate, which is characterized by a stress exponent of 3–5. There are further creep deformation mechanisms, which are described in detail in the relevant literature [16, 17].

To determine the stress exponent, n, and the apparent activation energy for creep Q_c, at least three tests at similar temperature but with different stresses (Fig. 9c) and three tests at similar stress but different temperatures (Fig. 9d) have to be carried out. The minimum creep rate, $\dot{\varepsilon}_{min}$, is determined for each test. From the plot log $\dot{\varepsilon}_{min}$ versus log σ, the stress exponent, n, is determined by linear regression (Fig. 9e). Note

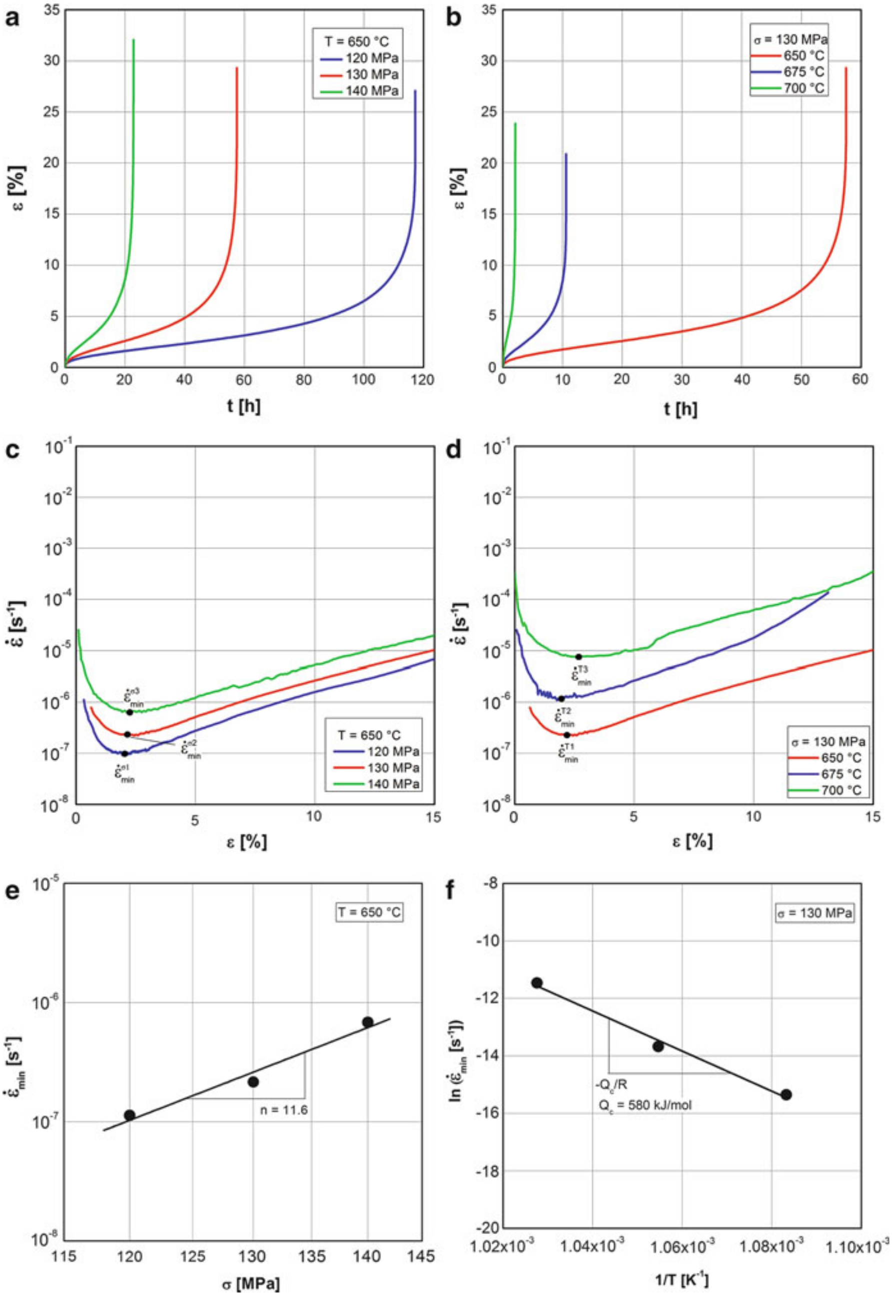

Fig. 9 Representation of a test series on heat-resistant steel P91 to demonstrate the stress and temperature dependence of the minimum creep rate. (**a**) Creep strain versus time for tests at T = const. and different applied stresses, σ. (**b**) Tests at σ = const. and different temperatures, T. (**c**) Creep rate versus creep strain at T = const. (**d**) Creep rate versus creep strain at σ = const. (**e**) Plot of log $\dot{\varepsilon}_{min}$ versus log σ to determine the stress exponent, n. (**f**) Plot of ln $\dot{\varepsilon}_{min}$ versus $1/T$ to determine the apparent activation energy, Q_c

that the value of the stress exponent ($n = 11.6$) for technical materials (here, ferritic-martensitic heat-resistant steel P91) also deviates from that of pure metals. Similarly, the activation energy is obtained by plotting ln $\dot{\varepsilon}_{min}$ versus 1/T (Arrhenius plot, Fig. 9f).

7.4 Stress Rupture Testing

Stress rupture testing focuses on the time to failure under creep conditions. The obtained creep rupture strength is defined as the stress value at which the specimen fails after being loaded at a certain temperature and time. The data is typically presented in stress-rupture diagrams (Fig. 10). In these diagrams, the applied stress is plotted versus the time to rupture on a log-log scale, which allows directly reading off how long a material can withstand the loading in a particular application if operating stress and temperature are known.

Stress rupture tests are often carried out in multiple testing units which allow parallel tests on many specimens, thereby increasing laboratory capacity and reducing costs. Multiple testing units are especially used for long-term tests. A number of specimens are loaded in each line section (load train) under a defined test force. Within a section, test pieces of different diameter can be used to provide different stress levels in each specimen. Strain measuring devices are simpler compared to creep tests, e.g., dial gauges are used.

Only with such efficient testing approaches, it is possible to establish the large creep rupture data collections that are needed for certain long-term applications, mainly in the energy sector. Power plant materials need to be characterized in wide ranges of temperatures and stresses, leading to testing times up to 100,000 h and more to represent the real service life of components (Fig. 11). Long-term test data is prone to significant scatter, and it is therefore challenging to derive representative temperature lines (like the schematic ones displayed in Fig. 10) from the large data sets. Considerable efforts are spent on these analyses, involving the application of different standardized procedures and models [18].

Fig. 10 Schematic stress-rupture diagram showing the stress value causing failure after loading at temperatures T_1 to T_3 and different times

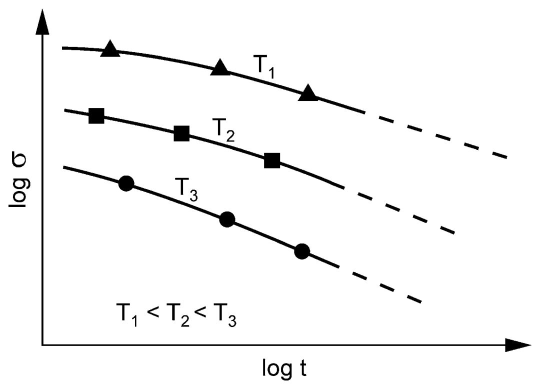

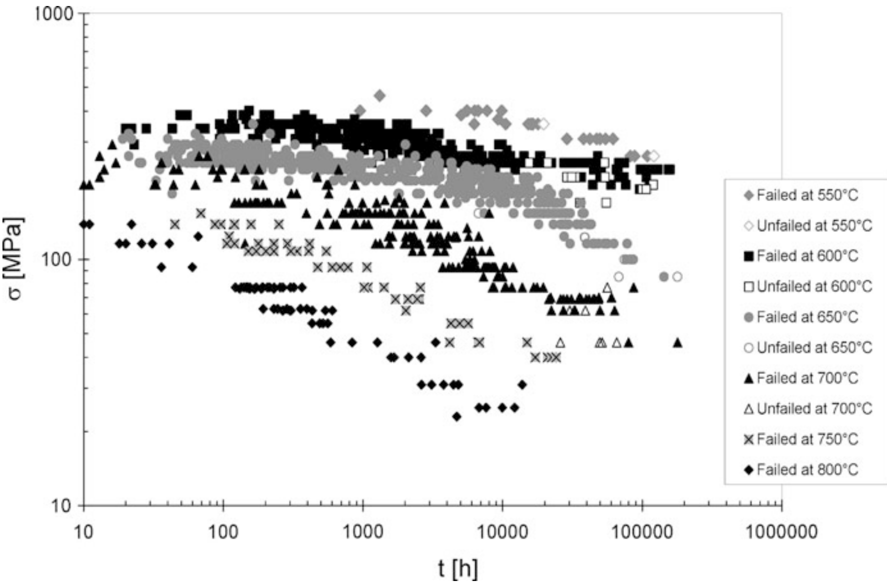

Fig. 11 Creep rupture strength of the austenitic heat-resistant steel Esshete 1250. (Data from Ref. [18])

8 Relaxation Tests

The phenomenon of stress relaxation at high temperatures is closely related to creep deformation since it relies on similar, thermally activated microstructural processes. Which of the phenomena will occur during a test is decided by the type of applied loading, namely, by the question whether load or strain is kept constant during the experiment. Creep tests involve constant force (or sometimes constant stress) conditions. This constantly applied load results in continuous dislocation movement and generation of plastic strain, eventually leading to rupture of the specimen (usually after considerable necking). Under constant strain conditions, plastic strains are similarly generated in the test piece at the beginning, but this growing plastic deformation simultaneously reduces the mismatch between the length of the specimen and the preset length (strain) under applied load. The more the specimen adapts plastically to this preset strain, the lower are the residual elastic strain and the stress in the specimen. The decrease or "relaxation" of the load also reduces the driving force for further dislocation movement. Therefore, stress relaxation behavior is characterized by pronounced load drops at the beginning, followed by more gradual further evolutions.

In technical applications, both constant load and constant strain loading regimes are of equal significance. Typical examples for constant load conditions in applications include pipes in the high pressure part of the steam cycle in thermal power plants. They are continuously subjected to a nearly constant steam pressure and thus exhibit gradual widening due to creep (unless any holders or connectors eventually

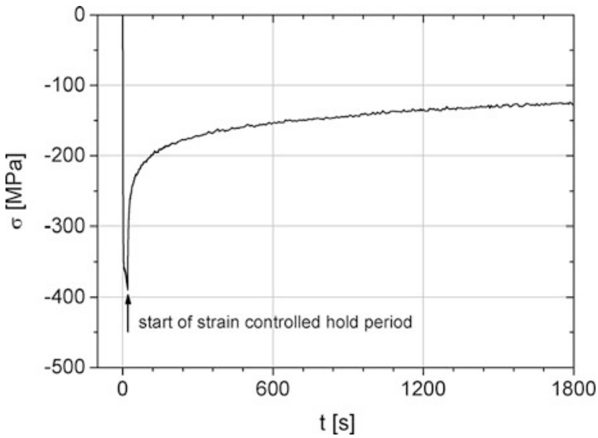

Fig. 12 Stress relaxation in a ferritic cast iron (GJS X SiMo 5.1) at 500 °C. The specimen was deformed to a compressive strain of 2% within 20 s and then kept under constant strain for 30 min

impede further deformation). Screw bolts of turbine housings are an example for parts, which undergo stress relaxation. The freshly tightened bolt experiences high tensile force/stresses, which in turn compress the parts of the housing and keep the turbine sealed. But already after little time-dependent elongation of the bolt, these clamping forces will reduce drastically. Its tensile stresses "relax," clearly an undesired behavior in this application.

Stress relaxation is already observed after purely elastic straining, but it similarly occurs after preloading to the plastic regime. In addition, it should be pointed out that relaxation behavior is not restricted to tensile loading. It equally occurs after compressive loading, as is demonstrated in Fig. 12. In this test, a ferritic cast iron was pre-deformed to 2% compressive strain within 20 s, resulting in a compressive stress of 390 MPa. The specimen was then kept under constant strain for 30 minutes, and the stress evolution was continuously recorded. After less than 100 seconds, stresses already fall below a value of 200 MPa. At the end of the test, almost two thirds of the initial stresses have "relaxed."

Dedicated relaxation tests can be performed either by subjecting specimens to strain-controlled holding in a mechanical test machine (for tensile loading, e.g., [19]) or by more technological approaches like model bolt joints which are exposed to temperature (e.g., [20]). The fast relaxation, which occurs during constant strain holding for several minutes or hours, is often also analyzed in complex cyclic test procedures for state-of-the-art parameter identification for deformation models (which typically combine load steps, repeated cycles, and hold periods at different strain levels and strain rates). Tests which aim at assessing the special damage behavior under combined dynamic and static loads (so-called creep-fatigue tests, e.g., in accordance to [21]) may also involve repeated hold times under strain control with respective relaxation responses.

Long-term relaxation tests under constant strain in testing machines should preferably be carried out in electromechanical screw-type machines, as hydraulic actuators inevitably impose small position oscillations on the test piece. Depending on the length of the hold period, special attention needs to be paid to the long-term stability of all involved sensors (temperature, strain, force). Their performance with regard to long-term drift should preferably be verified in pretests (e.g., by application of dead weights to the load cell, monitoring the extensometer reading while it is applied to a load-free specimen). Checking the zero point readings immediately after unloading and removal of the test piece can sometimes also help to identify drifting sensors.

9 Low Cycle Fatigue (LCF)

9.1 Basic Principles of the Test

In this test, the specimen is cyclically loaded by a constant mechanical amplitude at constant test temperature. The load can be applied in force or in strain control. In elevated temperature tests, mostly strain control is used with constant strain rate. The focus of the test is to study the behavior under strain-controlled fatigue loading combined with cyclic plasticity that causes failure after a low number of cycles (e.g., $<10^5$). Tests at high temperature may result in time-dependent strains (creep), which generally affect fatigue lifetime and the cyclic stress-strain behavior of a material. The total strain, ε_t, in a cycle is the sum of the elastic strain, ε_e, and the inelastic strain, ε_{in}. The inelastic strain has two components, the time-independent plastic strain, ε_p, and the time-dependent creep strain, ε_c:

$$\varepsilon_t = \varepsilon_e + \varepsilon_{in} = \varepsilon_e + \varepsilon_p + \varepsilon_c \tag{4}$$

Figure 13 schematically shows the characteristic values of stresses and strains of a stress-strain hysteresis curve. The size of the hysteresis curve is characterized by the total strain range, $\Delta\varepsilon_t$, and by the stress range, $\Delta\sigma$. Often, the plastic strain range is determined for further assessment of the cyclic deformation behavior. There are two options: the modulus for unloading following a peak tensile stress, E_T, and a peak compression stress, E_C, are determined and $\Delta\varepsilon_p$ is calculated from the difference $\Delta\varepsilon_t - \Delta\varepsilon_e$ (named $\Delta\varepsilon_p^t$ in Fig. 13a) [22]. Note that E_T and E_C are not the monotonic Young's modulus. They may change during the test due to changes in the microstructure. The second option uses the width of the hysteresis curve at mean stress (named $\Delta\varepsilon_p^w$ in Fig. 13a) [4]. It is sometimes difficult to determine E_T and E_C because at high temperature, the peaks of the hysteresis loop may show only a short linear part of the curve on unloading and the error in determining the slope might be large. In these cases, $\Delta\varepsilon_p^w$ can be established with higher accuracy and higher reproducibility.

Figure 13b shows a schematic hysteresis curve of a test with a hold time in compression. The major difference is the relaxation during the hold time, which results in a stress drop (named σ_{RC} in Fig. 13b).

Apart from test temperature, the test results depend on strain amplitude, ε_a, strain ratio, R_ε, cycle shape (e.g., triangle, sine), strain rate or frequency, and hold times. The strain ratio, R_ε, is defined as:

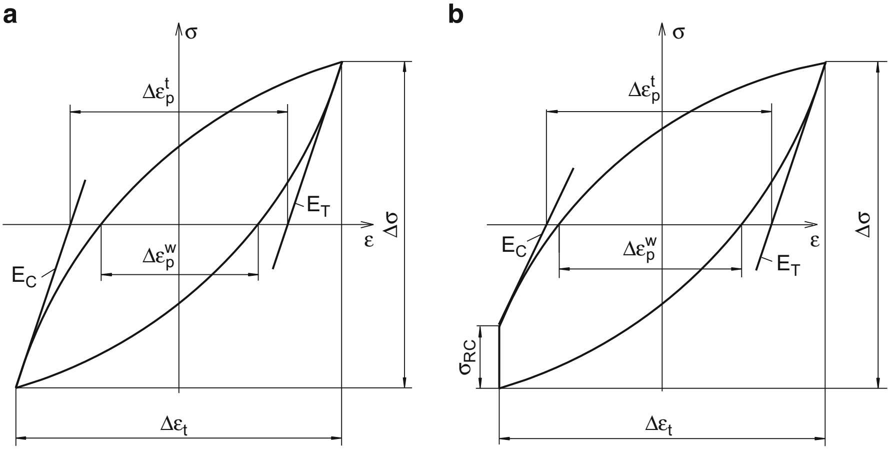

Fig. 13 Stress-strain hysteresis loop (schematic) with labeling of parameters and measured variables. (**a**) Continuous cycle without hold time, (**b**) cycle with hold time in compression

$$R_\varepsilon = \frac{\varepsilon_{min}}{\varepsilon_{max}} \tag{5}$$

Special attention should be paid to the alignment of the load train of the machine to minimize bending.

For the determination of reliable and consistent results, e.g., standard ISO 12106 [4] is applied, which describes the procedure for tests under alternating strain ($R_\varepsilon = -1$). The heating of the test piece shall be carried out without overshooting of the set temperature. Usually, resistance or radiation furnaces are used, but induction heating is possible as well, provided that the temperature gradient along the gauge length does not exceed 3 K. A generator with sufficiently low frequency is recommended to avoid the skin effect [4]. The temperature is controlled by a sufficient number of thermocouples, which are in close contact with the specimen surface, without falsifying the result by, e.g., initiating a crack at the point of contact. Frequently, thermocouples are attached by pressing, tying, or resistance spot welding (cf. Sect. 4). The latter should be avoided in the gauge length. Problems may arise even when welding to the radii if the material is notch sensitive. Before starting the test, the specimen must be held at test temperature for a sufficiently long time to assure complete heating through. The aforementioned standard does not give any specification for it. Other sources recommend 30 s/mm^2 cross section and a minimum time of 15 minutes. As creep effects need to be considered at high temperature, comparison of test results requires paying attention to the used frequencies or strain rates. It is recommended to use frequencies between 0.01 Hz and 1 Hz or strain rates between $5 \cdot 10^{-4}$ s^{-1} and $5 \cdot 10^{-2}$ s^{-1} [4].

9.2 Results on Austenitic Cast Iron

Results of test series of fatigue lifetime are often represented as total strain range $\Delta\varepsilon_t$ (or strain amplitude, ε_a) versus the number of cycles to failure, N_f. The failure criterion needs to be defined, i.e., N_f may represent, e.g., total separation of the specimen or a certain percentage change in the maximum tensile stress in relation to the level determined during the test [4]. An example is shown in Fig. 14 for a heat-resistant cast iron. In this case, N_f is defined as 20% stress drop. The plot shows that the lifetime decreases with increasing temperature. The temperature has a larger effect for this material above 600 °C due to thermal softening combined with time-dependent damage such as creep and oxidation. Hold times (open triangles) result in reduced lifetime due to additional damage caused by stress relaxation. Hold times in tension or compression in general may have different effects.

The hysteresis curves may provide information on possible changes of the stress-strain behavior during cycling. Figure 15 shows the first and the tenth cycle as well as the one at half lifetime for an austenitic cast iron at different temperatures. Fig. 15a shows that at 500 °C, there are distinct differences between the loops for the cycles at the beginning of the test and the one at half lifetime: the plastic strain decreases (i.e., the loop narrows; cf. Fig. 13a) and the peak stresses increase (especially the maximum stress), which is due to cyclic strengthening (cf. Fig. 16a). At 900 °C, there is only little change in the shape of the hysteresis curves (Fig. 15b); the width is almost unchanged. However, compared to 500 °C, the loop is much wider, although the strain amplitude is only a little higher. This reflects the increasing plastic strain with increasing temperature. In addition, the curves are less peaked at maximum and minimum strain. They are rather rounded out, which makes it more difficult to determine the slope (i.e., the modulus; cf. Fig. 13a) on unloading.

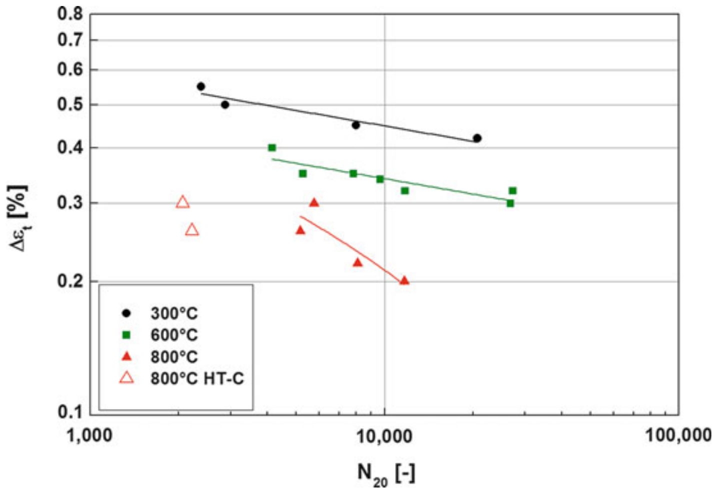

Fig. 14 Lifetime of GJS X SiMo 4.05. Total strain range, $\Delta\varepsilon_t$, versus no. of cycles to 20% stress drop, N_{20}, with and without hold time (180 s) at test temperatures between 300 °C and 800 °C (HT-C: hold time in compression)

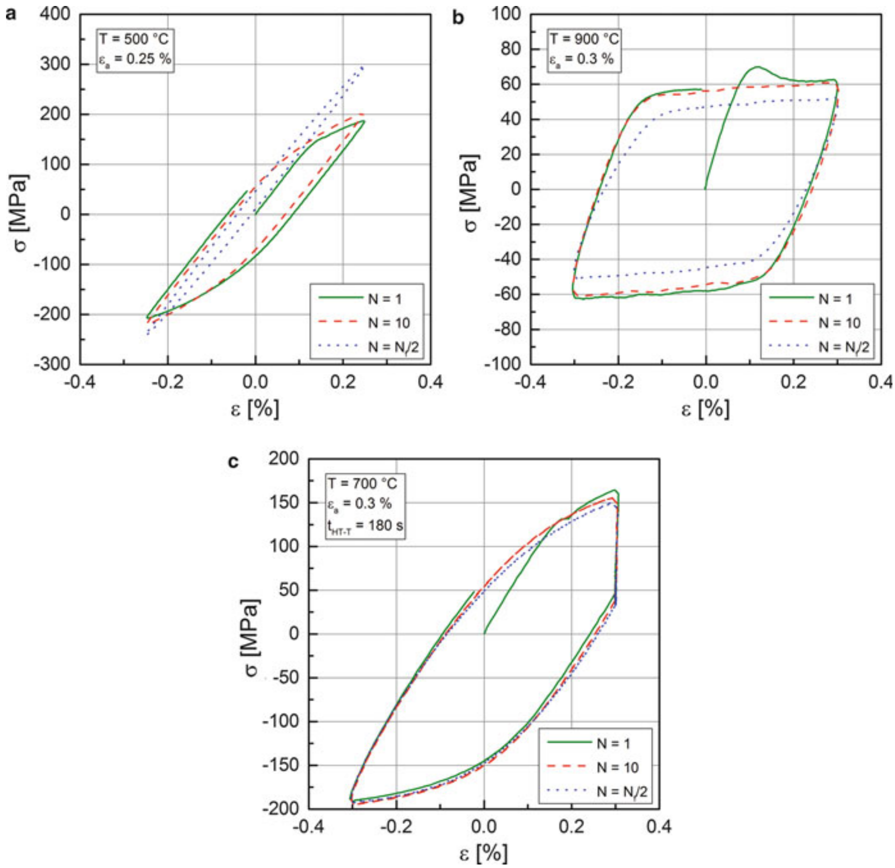

Fig. 15 Stress-strain hysteresis curves of LCF tests of austenitic cast iron Ni-Resist D5S, (**a**) $T = 500$ °C, $\varepsilon_a = \pm\ 0.25\%$, $N_f/2 = 39{,}228$, (**b**) $T = 900$ °C, $\varepsilon_a = \pm\ 0.3\%$, $N_f/2 = 800$, (**c**) $T = 700$ °C, $\varepsilon_a = \pm\ 0.3\%$ with 180 s hold time in tension (HT-T), $N_f/2 = 273$

At this high temperature, cyclic softening is observed, i.e., the peak stresses decrease with an increasing number of cycles (cf. Fig. 16b). Finally, Fig. 15c shows the hysteresis curves of a test at 700 °C with a hold time of 180 s in tension. The stress relaxation during the hold time is clearly visible. Its amount remains almost unchanged during cycling. It is striking that the hold time results in the development of a mean stress ($\sigma_{mean} = (\sigma_{max} + \sigma_{min})/2$) already in the first cycle, which is not the case for the tests without hold time.

The stress-strain response may change during cycling (cf. Fig. 15) due to microstructural changes caused by the plastic deformation. A material may undergo cyclic hardening or cyclic softening or it remains cyclically stable. This can be visualized on plotting the maximum and minimum stress versus cycle number, N. The evolution is temperature dependent (Fig. 16). Figure 16a shows, for an austenitic cast iron, that the behavior is characterized by cyclic hardening at the lower testing temperatures (20 °C and 500 °C).

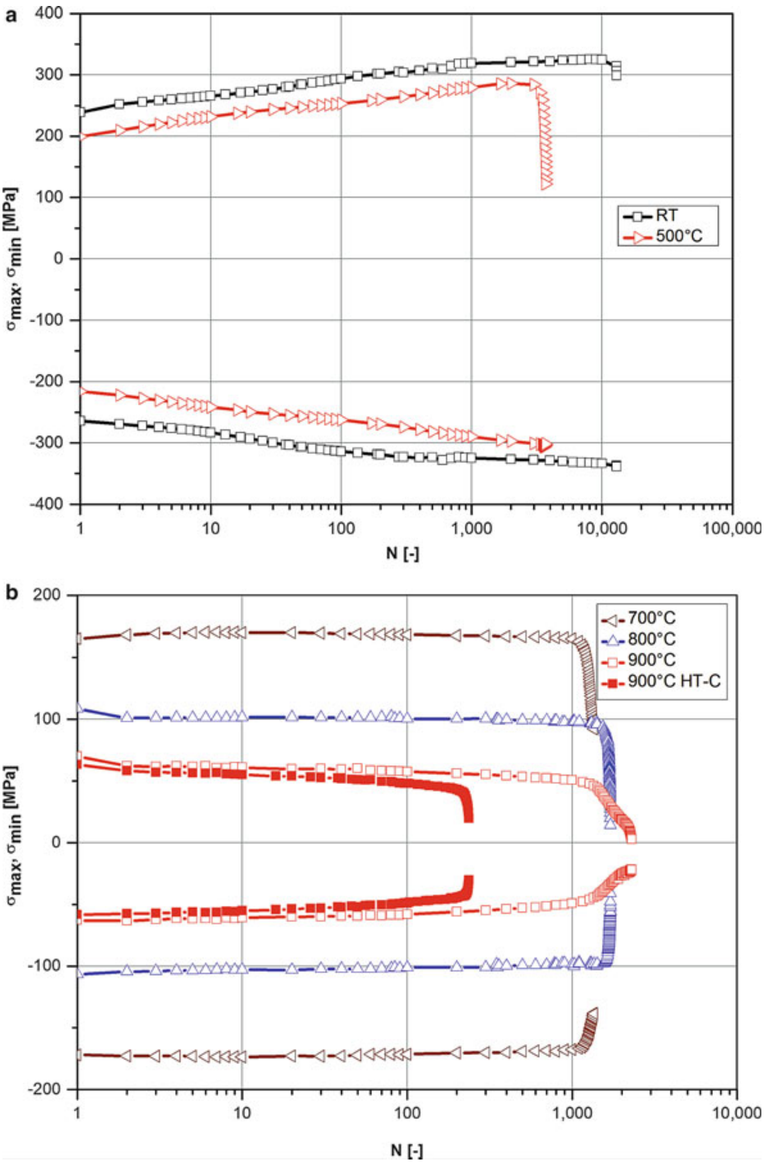

Fig. 16 Response of Ni-Resist D5S to strain cycling. Maximum and minimum stress versus no. of cycles, N. (**a**) $T = 20$ °C, 500 °C, $\varepsilon_a = 0.35\%$; cyclic strengthening. (**b**) $T = 700$ °C, 800 °C, 900 °C, $\varepsilon_a = 0.30\%$; HT-C = 180 s hold time in tension; visible cyclic softening at 900 °C

In contrast, at higher testing temperatures (700 °C, 800 °C, and 900 °C), the stresses either remain constant or show slight cyclic softening (Fig. 16b). The diagram also shows that a hold time reduces both the cyclic stresses and the lifetime in this case.

10 Thermomechanical Fatigue (TMF)

10.1 Basic Principles of the Test

The investigation of superimposed cyclic thermal and mechanical loads with arbitrary phase angles becomes more and more important for designing components that are subjected to thermal gradients, e.g., turbine blades, turbocharger housings, or exhaust manifolds. Materials exposed to such loads are in many cases investigated using TMF tests.

The TMF test represents an advancement of the LCF test. Therefore, a fundamental knowledge of the test procedure and the data analysis of the LCF test is presumed. The substantial difference to the LCF test is the varying temperature. In a TMF test, the specimen is subjected to a cyclic mechanical load as well as to a temperature cycle. Special attention has to be paid to the correct phasing between mechanical load and temperature, which is defined by the phase angle, φ.

In a strain-controlled test (TMF tests in force control are rarely performed), the sum (total strain, ε_t) of mechanical (ε_m) and thermal strain (ε_{th}) is set as a control value at any time during the test (Fig. 17). The mechanical strain has an elastic (ε_e) and a plastic (ε_p) component:

$$\varepsilon_t = \varepsilon_m + \varepsilon_{th} = \varepsilon_e + \varepsilon_p + \varepsilon_{th} \tag{6}$$

Often hold times are introduced to simulate stationary operating conditions of a component.

The anisothermal TMF test is characterized by cycling the temperature between a maximum (T_{max}) and a minimum temperature (T_{min}). The phase angle, φ, describes the time-based behavior between temperature and mechanical strain and remains unchanged during the test. However, as a test parameter, φ may vary between $\pm 180°$. It represents different loading conditions of the component. Typical values of φ are:

- $0°$ in-phase (IP): maximum and minimum of mechanical strain and temperature occur at the same time (Fig. 18a)
- $180°$ out-of-phase (OP): maximum of mechanical strain and minimum of temperature occur at the same time, and vice versa (Fig. 18b)
- $90°$: temperature is $90°$ ahead of mechanical strain (Fig. 18c)
- $-90°$: temperature is $90°$ behind of mechanical strain (Fig. 18d)

However, arbitrary other values of φ are possible.

The starting point of a TMF test is also a test parameter and may affect the test result. Usually, IP and OP tests start at T_{mean} and with $\varepsilon_m = 0$. OP tests with $\varphi \neq 180°$ often start at T_{min} with the corresponding mechanical strain (cf. Fig. 18c and d).

The typical number of cycles to failure of anisothermal TMF tests is comparable to isothermal LCF tests, i.e., $< 10^5$ cycles. It is recommended to apply the actual standards [5, 6] to determine reliable and consistent results. Similar to LCF tests, the alignment of the load train is of high importance for the determined lifetimes. TMF tests require a

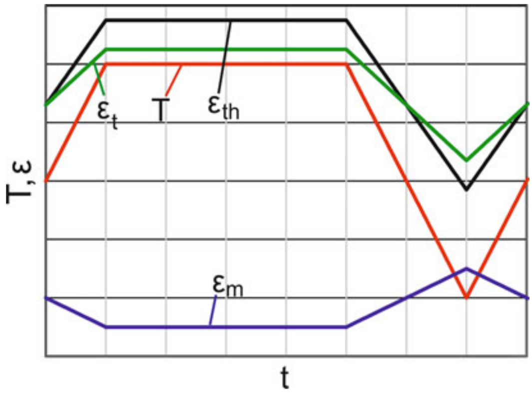

Fig. 17 Schematic representation of the different strain components in an out-of-phase (OP) test with hold time

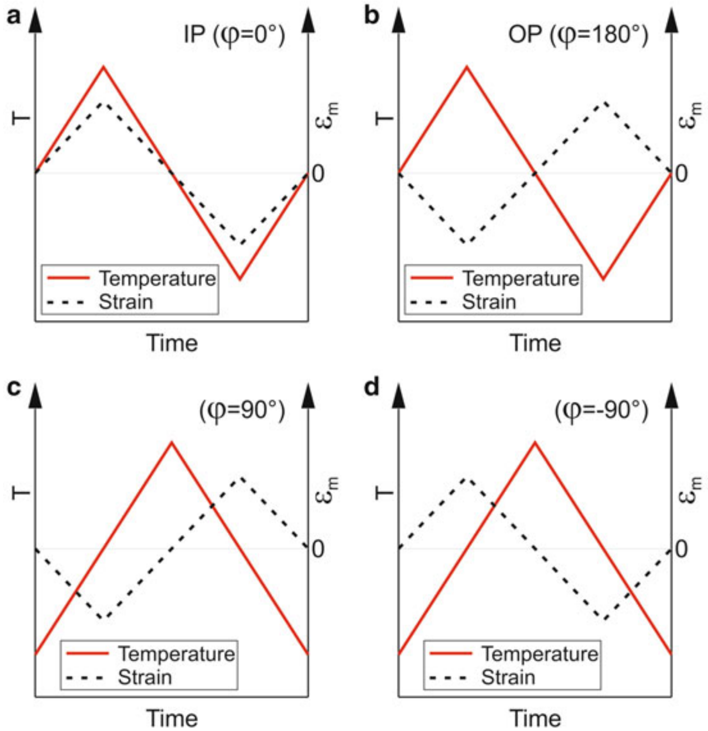

Fig. 18 TMF tests with different phase angles, φ, between temperature and mechanical strain: (**a**) in-phase test (IP; $\varphi = 0°$), (**b**) out-of-phase test (OP; $\varphi = 180°$), (**c**) 90° out-of-phase ($\varphi = 90°$), (**d**) $-90°$ out-of-phase ($\varphi = -90°$)

heating system, which allows establishing the aspired heating and cooling rates. Usually, induction heating or lamp furnaces are used. The cooling by natural convection and by heat flow into the cooled grips can be accelerated by blowing air to the specimen surface, which however may result in radial temperature gradients.

A parameter of particular importance is the temperature cycle, which should be as accurate as possible. The maximum temperature deviation from the set value should be $\leq$5 K for the entire cycle. Temperature gradients must be observed in axial as well as in circumferential direction. Radial gradients should be considered as well, especially when applying high temperature rates. Using bulk specimens and temperature rates >5 K/s may result in considerable radial temperature gradients and, consequently, thermal stresses [1], which may affect experimental lifetimes. Radial temperature gradients can be reduced by using hollow specimens. However, this results in lower lifetimes than in bulk specimens due to the larger surface.

A number of pretests have to be carried out to verify the correct test setup before the actual test is started. This includes the determination of Young's modulus, $E = f(T)$, and the thermal strain as a function of temperature, the optimization of the temperature path (to minimize temperature errors), and a zero stress test. The latter allows checking the accuracy of thermal strain compensation. The zero stress test is carried out under total strain control at $\varepsilon_m = 0$, i.e., $\varepsilon_t = \varepsilon_{th}(T)$. The resulting extreme values of stress reading occurring during zero stress test shall not exceed the limits defined by the respective standards.

10.2 Examples of Results on Heat-Resistant Cast Iron

Figure 19 shows the TMF lifetime of a ferritic heat-resistant cast iron at thermomechanical loading as total mechanical strain range, $\Delta\varepsilon_m$, versus the number of cycles to 20% stress drop, N_{20}, for different temperature ranges, ΔT, and different phase angles (IP, 180° OP, −90° OP). The minimum temperature is 300 °C in all tests; the maximum temperature is either 600 °C (circles), 700 °C (squares), or

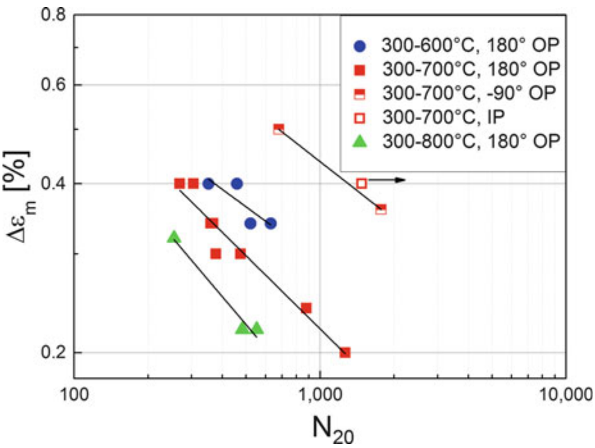

Fig. 19 TMF lifetime of GJS X SiMo 4.05 at thermomechanical fatigue with a hold time of 180 s at T_{max}. Total mechanical strain range, $\Delta\varepsilon_m$, versus no. of cycles to 20% stress drop, N_{20}, for different cycle types

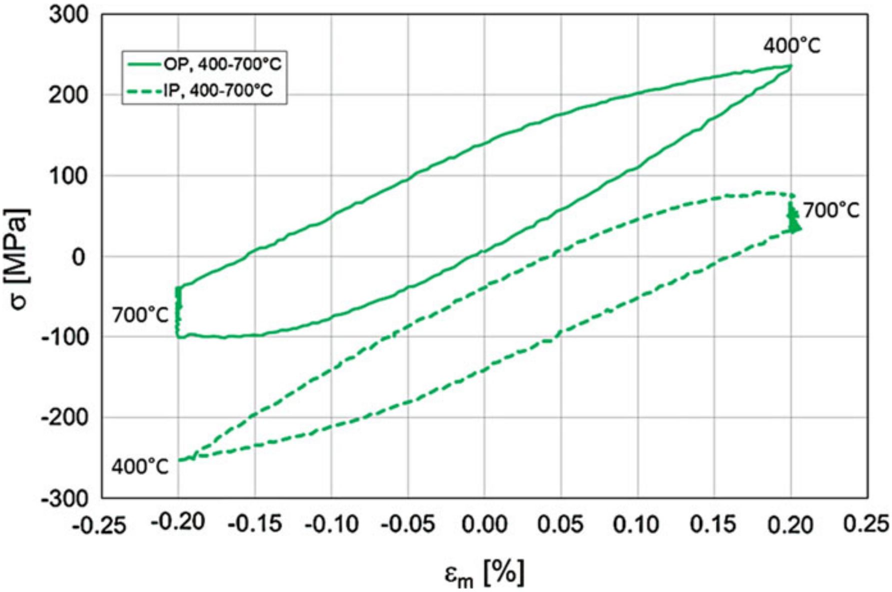

Fig. 20 Hysteresis curve of an IP and 180° OP-TMF test at half lifetime ($N_f/2$). $\varepsilon_m = \pm 0.2\%$, hold time of 180 s at T_{max}; Ni-Resist D5S

800 °C (triangles). The three curves in the lower left (full symbols) represent the 180° OP tests. The OP results show the highest lifetimes at the lowest maximum temperature (600 °C, circles) and the lowest lifetimes at the highest maximum temperature (800 °C, triangles). The reason is the increasing creep and oxidation damage with increasing temperature for this material. The loading paths IP (open square) and −90° OP (half open squares) are found further to the right and obviously result in lower damage and therefore longer lifetimes.

It is well known that damage can evolve differently during TMF testing. In some materials, IP loading is more damaging than OP loading, and it can be the opposite in others. Creep, fatigue, and oxidation processes provide the main contributions to damage. The type of material investigated as well as the applied loading conditions determines their individual contributions and their mutual interactions. According to Nitta and Kuwabara [23], the behaviors can be classified as follows:

(i) The combination of high temperature and tensile stresses during IP loading is more detrimental than OP loading: creep damage dominates.
(ii) Surface oxidation leads to embrittlement; crack initiation takes place early if high tensile loads are accompanied by low temperatures: lifetime under OP loading is more damaging.
(iii) Lifetime is about the same because neither environmental effects nor creep damage dominates.

Similar to LCF tests, the stress-strain hysteresis loops are often plotted for further analysis. Figure 20 shows an example for an austenitic cast iron. The two curves represent results of two tests in the same temperature range (400–700 °C) but with different phasing. The continuous curve represents a 180° OP test and the broken line an IP test with the same mechanical strain amplitude of ±0.2% and a hold time at T_{max}. It is clearly visible that the stress response is quite different: the OP test shows a higher maximum tensile stress and a lower minimum compression stress as the IP test. The mean stress is tensile for the OP and compressive for the IP test. It is also evident that the stresses relax during the hold times at 700 °C in both cases.

11 Fatigue Crack Propagation

In this test, the fatigue crack growth rate is determined in a region of the stress intensity factor range, ΔK, from the threshold, ΔK_{th}, to the onset of unstable crack propagation. ΔK is defined by the linear elastic fracture mechanics theory [24, 25]:

$$\Delta K = \Delta\sigma\sqrt{\pi a} \cdot Y \tag{7}$$

$\Delta\sigma$ is the stress range, a the crack length, and Y a function that depends on the specimen and crack geometry. The results are interpreted as the resistance of a material to subcritical crack extension under cyclic force. They are used for [26, 27]:

- Investigating the influence of fatigue crack growth on the predicted life of a component
- Evaluating the crack growth resistance of a material or heat-treat condition
- Establishing material selection criteria and inspection requirements
- Defining the requirements of NDT testing
- Macroscopic quantitative determination of various factors (e.g., load, microstructure, manufacture)

In this test, a precracked notched specimen is subjected to a cyclic force. The crack length, a, is measured as a function of the number of cycles, N. The fatigue crack growth rate da/dN is calculated and expressed as a function of the stress intensity factor range, ΔK:

$$\Delta K = K_{max} - K_{min} = (\sigma_{max} - \sigma_{min})\sqrt{\pi a} \tag{8}$$

Stress ratio, R_σ, temperature, and environments may affect the fatigue crack growth rate significantly.

At low temperature and high cycle frequency, the crack growth rate is cycle dependent and can be described by the empirical crack growth law (Paris law):

$$\frac{da}{dN} = C\Delta K^m, \tag{9}$$

with C and m being constants.

At very high temperature and low frequency, fracture mechanisms may become time dependent and they may be controlled by thermally activated creep and/or environmental processes. If the inelastic zone at the crack tip reaches a substantial fraction of the specimen dimension, the limits of linear elastic fracture mechanics are no longer valid and different approaches have to be applied (using parameters like C^*, $C(t)$, C_t) to take time dependence into account [28–30].

There are standard specimen geometries, which may vary in size. Common specimen types as shown in Fig. 21 are, e.g., compact tension (CT), center cracked tension (CCT), or single edge notch tension (SENT) [31]. For aerospace applications, the corner-crack specimen (CC) with square or rectangular cross section is often used, because it reflects the geometric situation in components where the cracks usually appear at a corner, such as in holes in turbine disks [26]. The CC specimen may be loaded in tension and compression for positive and negative R_σ-values. Due to its geometry (which is comparable to LCF test pieces with respect to total dimension), it easily fits into standard radiation furnaces and uses similar grips.

After producing a notch (depending on material, e.g., by using electric discharge machining, grinding, diamond saw, laser) of approximately 0.1 mm depth in the center of the reduced section, a fatigue precrack is produced at the root of the notch by cyclic loading to provide a sharp and straight fatigue crack of sufficient depth. The growth of the crack is monitored. A common technique is the potential drop method, which is also suitable at high temperature (details are described in the standards [26, 27, 31]). The compliance method is applied as well [27]. It is essential for both methods to assure that the temperature field is uniform and constant because temperature changes may result in false indications of crack length change. As the

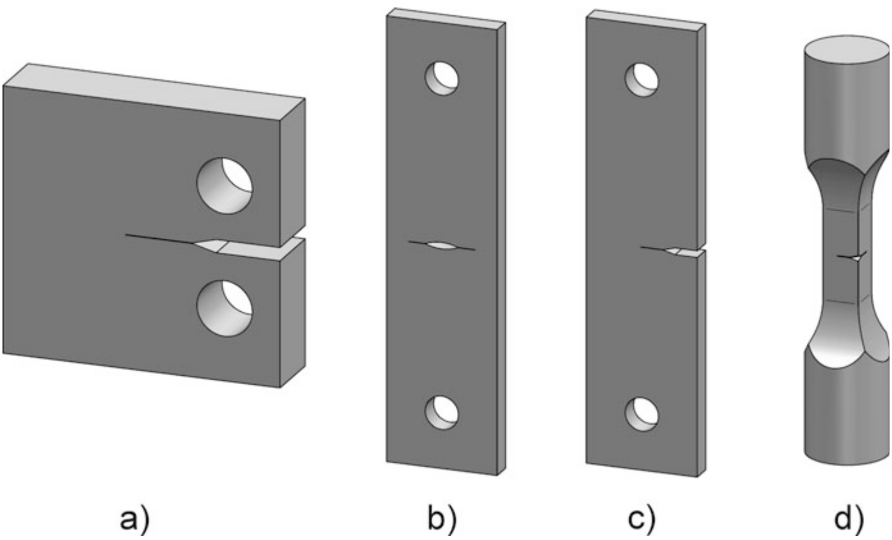

Fig. 21 Examples of standard specimen geometries for crack growth testing: (**a**) compact tension (CT), (**b**) center cracked tension (CCT), (**c**) single edge notch tension (SENT), (**d**) corner crack (CC)

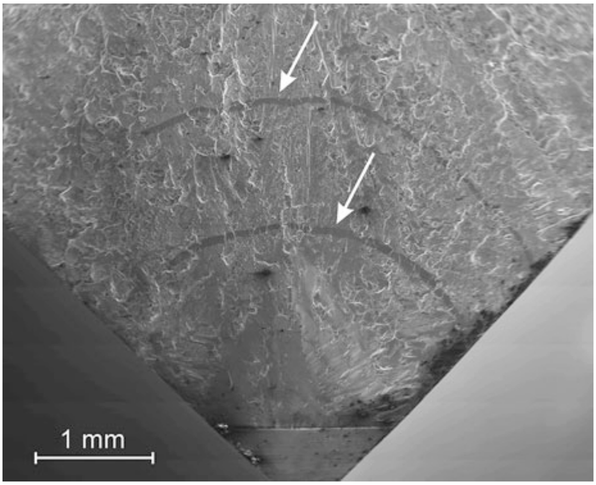

Fig. 22 Beach marks on the fracture surface of a Ni-base alloy

crack grows, the applied force range is maintained or reduced in a controlled manner until the crack is of sufficient depth.

Then the actual crack growth test is started. The maximum and minimum force maintain constant, and ΔK is allowed to increase with crack extension. The crack depth is recorded as a function of a number of cycles by potential drop or by compliance method. From these signals, the evolution of the crack length versus the number of cycles is determined analytically. A correction of the calculated length for individual specimen/crack front characteristics is made by creating so-called beach marks on the fracture surface during the crack growth test. They are introduced by periods of a few thousand cycles with the same K_{max} but with different R_σ-ratio and/or different frequency. An example is shown in Fig. 22. Beach marks are measured at the end of the test and they serve the calibration of the crack length curve calculated from the potential drop signal or from the change of compliance. After a numerical analysis of the recorded data, the crack growth rate log(da/dN) is plotted as a function of log (ΔK). The crack growth threshold, ΔK_{th}, represents the asymptotic value of ΔK for da/dN converging zero (usually defined as 10^{-8} mm/cycle [31]).

A machine with a feedback load-controlled servohydraulic or electromechanical system is required designed for smooth loading without exceeding the desired maximum force. It should be able to stop cycling at desired crack depth measured as potential level or compliance. Similar to LCF tests, the alignment of the load train is of high importance. The thermocouple should be in close contact with the test piece, at the centerline of one face adjacent to the notch, 2 mm to 4 mm above or below the crack plane [26]. Requirements with respect to temperature deviations must be fulfilled. Usually, radiation furnaces are used to heat up the test pieces and the grips. At very high temperatures (1000 °C and above), strength limits of the grips might be exceeded and induction heating can be a better choice. However, the interference of the induction field and the potential drop signal may affect the quality of the crack growth data.

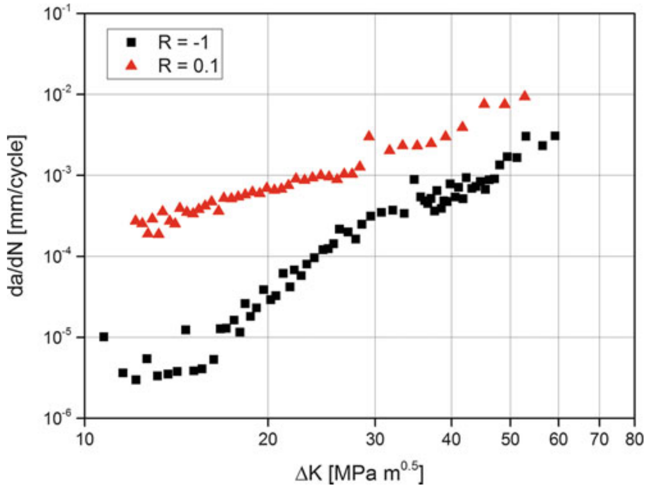

Fig. 23 Crack growth, da/dN, versus stress intensity factor range, ΔK, at 950 °C for a Ni-based superalloy and different load ratios, R_σ

Figure 23 shows da/dN–ΔK curves as a function of the load ratio, R_σ, for a Ni-based superalloy at 950 °C. The results show that the crack growth in tests with $R = 0.1$ is about one order of magnitude higher than with $R = -1$.

12 Additional Considerations

In addition to the before-mentioned specific aspects of different test types, a number of general factors should be considered that can seriously affect high temperature test results.

High temperature tests are often performed in larger test series, e.g., to generate data for calibrating mechanical models. Consequently, the testing programs usually cover a wide range of temperatures from room temperature to the highest service temperature. Whenever possible, it is advisable to perform all tests on the same test rig(s) to avoid additional error sources. However, high temperature materials tend to exhibit high strengths and poor ductility at low temperatures while exhibiting opposite behavior at high temperatures. A number of issues arise from this pronounced change of deformation characteristics:

(i) Careful choice of the involved sensors is imperative to be able to record all desired information. Especially regarding the test forces, the pronounced loss of strength under static (cf. Fig. 6) but mainly under cyclic loading (cf. Fig. 15) may result in stresses of only few megapascals at high cycle numbers. It should be carefully reviewed whether the data obtained in such cases may still be considered since they may fall outside the calibrated range of the used force transducer.

(ii) When specimens are “soft” at high temperature, they may become extremely sensitive to extensometer forces. High temperature extensometers are often pressed to the specimen by a spring load which applies a low radial force to the gauge section of the specimen. When interacting with a "soft" specimen, these forces may be sufficient to induce nonuniform deformation resulting in bending of the specimen (cf. Fig. 24).

(iii) Test rigs may fail to meet the allowable alignment tolerances especially at low forces, as the straightening effect of the applied load is then negligible.

(iv) An adaption of the control parameters is typically necessary when material characteristics are changing. It is strongly recommended to carefully check the test machine's performance at each test temperature.

(v) Phenomena like drift of sensors, sliding in the grips, loss of contact due to oxidation may occur at certain temperatures only. Careful revision and intercomparison of the test results is therefore advisable, but not easy due to the aforementioned pronounced changes of material behavior. It is recommended to continuously record the crosshead or piston position signals and, if applicable, the heating power output in addition to the standard signals (i.e., force, strain, temperature). The additional data can be helpful in identifying potential troubles that occurred in the testing process.

If adaptions of the experimental setup to different load levels are not possible, e.g., due to unavailability of alternative sensors, it may sometimes be helpful to adjust the specimen dimensions by enlarging the cross sections. However, it should be considered

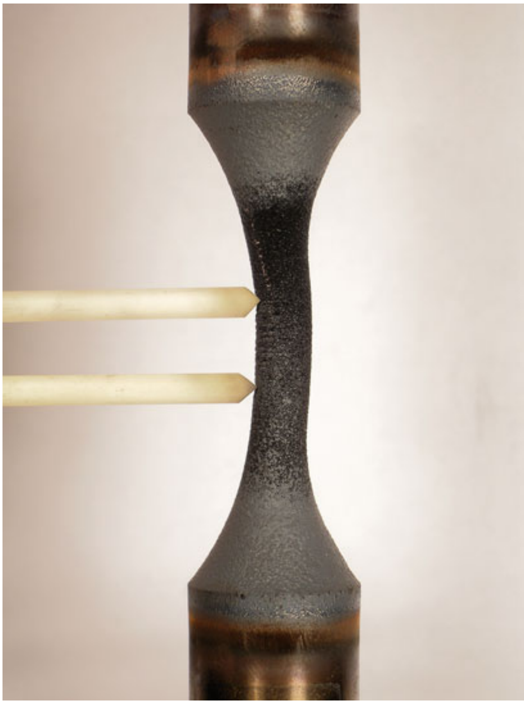

Fig. 24 Nonuniform deformation of a specimen due to extensometer contact forces after testing at very high temperature

that changes in the aspect ratio (length to diameter) of the gauge section will have an impact on the test results. Therefore, all aforementioned test standards include mandatory requirements regarding test piece geometries. Larger cross sections will result in longer gauge sections. These can facilitate reaching a homogeneous temperature profile if "cold" grips are used (cf. Sect. 2), but may also represent a further complication since adequate heating equipment (larger furnace, longer induction coils, etc.) is then required.

The sizes of test pieces generally need to be adapted to the type of material that is tested. High grain-size materials may require larger cross sections to establish better averaging of the properties, whereas single crystal materials are often not available in the desired dimensions, inevitably leading to testing of small specimens. These, in turn, will again promote all before-mentioned issues related to low test loads. Further effects of small specimen sizes on the obtained deformation characteristics have been reported for diffusion-controlled (creep) deformation (e.g., [32, 33]).

Testing of small specimens is not recommended whenever significant oxidation of the material is expected. Material loss at the surface is then an issue in all long-term tests (consider that even for a short tensile test, the heating procedure may take several hours). Surface oxidation then decreases the load-carrying cross section, and this process is clearly more pronounced the smaller the test piece is. Testing of larger diameter specimens is therefore recommended but will not necessarily avoid all oxidation influences, since different interactions of oxidation and deformation have been reported [34]. These include, e.g., early formation of cracks when cracks from the less-strain-tolerant oxide layer induce stress concentrations at the oxide/substrate interface. Cracks may similarly start at corrosion pits that have formed at the specimen's surface. Crack propagation can also be strongly influenced if air gets access to the crack tip and local plasticity and oxidation act simultaneously.

However, in many cases, much more basic interactions will affect the obtained test results. Oxide layers tend to detach from the strained specimens after reaching a certain thickness, producing errors in the strain and temperature signals if contacting measurement techniques are used. Thermocouples may completely fall off the specimen, leading to serious overheating of the test piece and possibly damage of the heating equipment. The use of non-contacting measurement methods like pyrometers and optical extensometers is unfortunately of little advantage, since they would equally analyze the detaching oxide layer, which neither exhibits the actual strain nor temperature of the substrate material below.

Complementary tests in controlled atmosphere (vacuum or inert gases) can be very helpful to assess the impact of material-environment interactions, but the test conditions are then less representative for real working conditions of the material in applications. Again, a careful and critical review of procedures and obtained results is mandatory to avoid wrong conclusions on the material's properties.

Acknowledgments Thanks are due to Mike Spindler at EDF Energy Generation for providing the creep rupture data in Fig. 11. All other data in this chapter were generated at the authors' institute. We would like to thank the following colleagues who provided research results and photographs, or prepared drawings and diagrams: Anja Archie, Bernard Fedelich, Andreas Hamann, Ole Kahlcke, Georgia Künecke, Peter Löwe, Kathrin Matzak, Sina Schriever, Elke Sonnenburg, and Patrick Uhlemann.

References

1. Hähner P, Affeldt E, Beck T, et al. Validated Code-of-Practice for Strain-Controlled Thermo-Mechanical Fatigue Testing. 92-79-02216-4, European Commission, Petten, NL; 2006.
2. ISO 6892-1: Metallic materials - Tensile testing - Part 1: Method of test at room temperature. International Organization for Standardization. Geneva: International Organization for Standardization; 2017.
3. ASTM E1012: Standard Practice for Verification of Test Frame and Specimen Alignment Under Tensile and Compressive Axial Force Application. West Conshohocken: ASTM International; 2014.
4. ISO 12106: Fatigue testing – Axial-strain-controlled method. Geneva: International Organization for Standardization; 2017.
5. ISO 12111: Fatigue testing – Strain-controlled thermomechanical fatigue testing method. Geneva: International Organization for Standardization; 2011.
6. ASTM E2368: Standard Practice for Strain Controlled Thermomechanical Fatigue Testing. West Conshohocken: ASTM International; 2010.
7. ASTM E1875: Standard Test Method for Dynamic Young's Modulus, Shear Modulus and Poisson's Ratio by Sonic Resonance. West Conshohocken: ASTM International; 2013.
8. Beckmann J, Rehmer B, Finn M, et al. Determination of the elastic properties of solids – part 1 – comparative evaluation of different test procedures. Mat Test. 2006;48:274–81.
9. Fedelich B, Beckmann J, Finn M, et al. Determination of temperature dependent elastic constants of anisotropic materials by the resonance method. In: Proceedings of the Materials Week 2002. Munich: Werkstoff-Informationsgesellschaft; 2002.
10. ISO 6892-2: Metallic materials – Tensile testing – Part 2: Method of test at elevated temperature. Geneva: International Organization for Standardization; 2011.
11. ASTM E21: Standard Test Methods for Elevated Temperature Tension Tests of Metallic Materials. West Conshohocken: ASTM International; 2017.
12. ASTM E8/E8M: Standard Test Methods for Tension Testing of Metallic Materials. West Conshohocken: ASTM International; 2016.
13. ASTM E139: Standard Test Methods for Conducting Creep, Creep-Rupture, and Stress-Rupture Tests of Metallic Materials. West Conshohocken: ASTM International; 2011.
14. ISO 204: Metallic materials – Uniaxial creep testing in tension – Method of test. International Organization for Standardization; 2009.
15. Dieter GE. Mechanical metallurgy. London: McGraw-Hill Book Company; 1988.
16. Cadek J. Creep in metallic materials. Amsterdam: Elsevier; 1988.
17. Poirier J-P. Creep of crystals – high temperature deformation processes in metals, ceramics and minerals. Cambridge, UK: Cambridge University Press; 1985.
18. Spindler MW, Spindler SL. Creep deformation, rupture and ductility of Esshete 1250. Int J Pres Ves Pip. 2008;85:89–98.
19. EN 10319-1: Metallic materials – Tensile stress relaxation testing – Part 1: Procedure for testing machines. Brussels: European Committee for Standardization; 2003.
20. EN 10319-2: Metallic materials – Tensile stress relaxation testing – Part 2: Procedure for bolted joint models. Brussels: European Committee for Standardization; 2007.
21. ASTM E2714: Standard Test Method for Creep-Fatigue Testing. West Conshohocken: ASTM International; 2013.
22. ASTM E606: Standard Practice for Strain-Controlled Fatigue Testing. West Conshohocken: ASTM International; 2012.
23. Nitta A, Kuwabara K. In: High temperature creep fatigue. London: Elsevier; 1988. p. 203–22.
24. Anderson TL. Fracture mechanics: fundamentals and applications. Boca Raton: CRC Press; 2005.
25. Chowdhury P, Sehitoglu H. Mechanisms of fatigue crack growth – a critical digest of theoretical developments. Fatigue Fract Eng M. 2016;
26. EN 3873: Aerospace series – Test methods for metallic materials - Determination of fatigue crack growth rates using Corner-Cracked (CC) test pieces. Brussels: European Committee for Standardization; 2011.

27. ASTM E647: Standard Test Method for Measurement of Fatigue Crack Growth Rates. West Conshohocken: ASTM International; 2015.
28. Suresh S. Fatigue of materials. 2nd ed. Cambridge: Cambridge University Press; 2004.
29. Bassani JL, Hawk DE, Saxena A. Evaluation of the C_t parameter for characterizing creep crack growth rate in the transient regime. In: Saxena A, Landes JD, Bassani JL, editors. Nonlinear fracture mechanics: volume I – time dependent fracture, ASTM STP 995. Philadelphia: American Society for Testing and Materials; 1989. p. 7–26.
30. Landes JD, Begley JA. A fracture mechanics approach to creep crack growth. In: Rice JR, Paris PC, editors. Mechanics of crack growth, ASTM STP 590. Philadelphia: American Society for Testing and Materials; 1976. p. 128–48.
31. ISO 12108: Metallic materials — Fatigue testing — Fatigue crack growth method. Geneva: International Organization for Standardization; 2012.
32. Olbricht J, Bismarck M, Skrotzki B. Characterization of the creep properties of heat resistant 9–12% chromium steels by miniature specimen testing. Mater Sci Eng A. 2013;585:335–42.
33. Krompholz K, Kalkhof D. Size effect studies of the creep behaviour of a pressure vessel steel at temperatures from 700 to 900 °C. J Nucl Mater. 2002;305:112–23.
34. Cook RH, Skelton RP. Environment-dependence of the mechanical properties of metals at high temperature. Int Metal Rev. 1974;19:199–222.